A global climate model study of CH_4 emissions during the Holocene and glacial-interglacial transitions constrained by ice core data

S. L. Harder,[1] D. T. Shindell,[2] G. A. Schmidt,[2] and E. J. Brook[3]

Received 20 December 2005; revised 29 September 2006; accepted 11 October 2006; published 16 February 2007.

[1] Ice core records show atmospheric methane mixing ratio and interpolar gradient varying with climate. Changes in wetland sources have been implicated as the basis for this observed variation in the record, but more recently, modeling studies suggest that changes in the CH_4 sink resulting from changes in sea surface temperature (SST) and emissions of other volatile organic carbon (VOC) compounds by vegetation must also be considered. We use the Goddard Institute for Space Studies (GISS) General Circulation Model (GCM) with the GISS Tropospheric Chemistry Model to study the response of the methane mixing ratio to source changes during the Holocene and also to a changing chemical sink during glacial-interglacial transitions. We combine model results with ice core data to demonstrate a method that provides constraints on changes in northern and tropical methane sources. Results show that within the Holocene, changes in the atmospheric methane mixing ratio and latitudinal gradient are not linear with respect to changing methane emissions. Tropical and northern emissions varied from preindustrial levels by as much as 38% and 15%, respectively, within the Holocene. At glacial-interglacial transitions the methane mixing ratio is sensitive to changes in both VOC and tropical methane emissions and the sensitivity also depends strongly on the assumed SST shift. Our findings suggest that changes in the ice core methane record are likely the result of changes in both the source and the sink. Changes in the sink become especially important when changes in methane mixing ratio and/or climate are large.

Citation: Harder, S. L., D. T. Shindell, G. A. Schmidt, and E. J. Brook (2007), A global climate model study of CH_4 emissions during the Holocene and glacial-interglacial transitions constrained by ice core data, *Global Biogeochem. Cycles*, *21*, GB1011, doi:10.1029/2005GB002680.

1. Introduction

[2] Ice core records reveal that both the mixing ratio and latitudinal distribution of atmospheric methane (CH_4) have changed with climate throughout the last glacial cycle [*Chappellaz et al.*, 1990; *Brook et al.*, 1996; *Dällenbach et al.*, 2000]. These changes have been considered to reflect changes in terrestrial vegetation and ecosystems as regional temperature and soil moisture change. Wetlands are the dominant natural source of CH_4 and several modeling studies have attributed changes in the ice core record to changes in wetland production and distribution [*Khalil and Rasmussen*, 1987; *Chappellaz et al.*, 1993; *Crutzen and Brühl*, 1993; *Chappellaz et al.*, 1997; *Martinerie et al.*, 1995; *Brook et al.*, 2000; *Dällenbach et al.*, 2000]. More recently changes in the oxidation capacity of the atmosphere have also been implicated in CH_4 variability as well as changes in wetland extent resulting from encroaching ice sheets and changes in sea level for glacial-interglacial transitions [*Kaplan*, 2002; *Adams et al.*, 2000; *Valdes et al.*, 2005].

[3] Change in the latitudinal distribution of CH_4 emissions is reflected by the interpolar gradient (IPG), hereafter defined as $(N/S - 1) \times 100$, where N and S are surface mixing ratios over Greenland and Antarctica, respectively, expressed as the percent that N exceeds S. The gradient arises because extra-tropical anthropogenic and natural sources are much greater in the north than the south. While tropical emissions are mixed equally within both hemispheres, the asymmetry of higher-latitude emissions results in mixing ratios being greatest at high northern latitudes and decreasing gradually toward the southern pole. Changes in the IPG provide qualitative information about how northern and tropical emissions change relative to each other, a decrease in the ratio of northern to tropical emissions producing a decrease in the IPG, and opposite changes in the source distribution producing an increase in the IPG. Three-box model studies constrained by ice core data have been carried out to determine quantitative changes in tropical and northern methane emissions for specific periods during the Holocene and the last glacial cycle [*Chappellaz et al.*, 1997; *Dällenbach et al.*, 2000; *Brook et al.*, 2000].

[1]School of Earth and Environmental Sciences, Washington State University, Vancouver, Washington, USA.
[2]NASA Goddard Institute for Space Studies and Center for Climate Systems Research, Columbia University, New York, New York, USA.
[3]Department of Geosciences, Oregon State University, Corvallis, Oregon, USA.

0886-6236/07/2005GB002680

Results suggest that changes in tropical emissions were primarily responsible for changes in mixing ratio within the Holocene while northern along with tropical emission changes were important at glacial-interglacial and stadial-interstadial transitions.

[4] More recently ecosystem modeling studies of *Kaplan* [2002] suggest that changes in wetland CH_4 emissions may not solely account for the larger glacial-interglacial changes in atmospheric mixing ratio. They suggest that a change in the primary sink, oxidation by hydroxyl radical (OH), might explain the magnitude of the change in CH_4 mixing ratio. The availability of OH for methane removal depends on production and the abundance of competing reactive compounds, both of which are sensitive to climate. Vegetation emissions of volatile organic compounds (VOCs) have been proposed as a possible competitor. *Adams et al.* [2000] used reconstructions of vegetation biome distributions for the Holocene and LGM calculating VOC emissions on the basis of leaf area index, foliage emission rate, and canopy temperatures. They found a decrease for global VOC emissions of almost 60% from the preanthropogenic Holocene to LGM conditions for a tropical surface temperature decrease of 5°C. *Valdes et al.* [2005] used a GCM with a dynamic vegetation model to explore changes in VOC and CH_4 emissions between the Preindustrial Holocene (PI, circa 1700 AD) and the last glacial maximum (LGM). They found greater sensitivity of VOC emissions to temperature, their simulation producing a 50% decrease in emissions for a 1°C tropical surface temperature decrease. Northern CH_4 emissions also decreased by 50% but tropical CH_4 emissions decreased only 3%, suggesting that the increased tropical OH sink combined with the decline in northern emissions were large enough to account for the change in CH_4 mixing ratio with very little change in tropical CH_4 emissions. However, LGM surface temperature distribution is not well established and may have been colder than the 1°C drop indicated by CLIMAP (1981) [*Broecker*, 1985; *Crowley*, 1995; *Webb et al.*, 1997; *Kucera et al.*, 2005]. These results underscore the importance of understanding the sensitivity of vegetation, wetland emissions, and OH production to temperature.

[5] Here we use the GISS GCM, ModelE, with the tropospheric chemistry model to address the following questions: (1) What is the sensitivity of CH_4 mixing ratio and IPG to changes in tropical and northern emissions throughout the PI Holocene? (2) What is the sensitivity of CH_4 mixing ratio to VOC emissions and climate? (3) What changes in emissions are consistent with both the ice core CH_4 record and predicted changes in the sink? To address these questions we perform sensitivity studies testing the response of CH_4 mixing ratio to changes in tropical and northern CH_4 emissions, and global VOC emissions. We combine modeled results with ice core data to produce plausible changes in emissions distributions for specific periods within the Holocene. We then explore the sensitivity of CH_4 mixing ratio to changing VOC and tropical CH_4 emissions for glacial to Holocene transitions. The response of the mixing ratio is then tested using four different climatologies, the first representative of an SST change consistent with a decline in North Atlantic Deep Water formation, as has been hypothesized for the Younger Dryas [*Rind et al.*, 2001] and 3 increasingly cooler scenarios for the LGM. Results are discussed regarding changes in the oxidation capacity of the atmosphere and the interpretation the ice core CH_4 record. Another potentially significant CH_4 source, clathrates, is not addressed here. Although there is evidence of past continental shelf collapse which may have periodically led to significant increases in CH_4 emissions at climate transitions [*Maslin et al.*, 2004], there is currently no evidence from ice core data of catastrophic CH_4 release over the last 50,000 years [*Brook et al.*, 2000; *Sowers*, 2006; *Schaefer et al.*, 2006].

2. Model Description

2.1. Climate Model

[6] The model used is the GISS GCM, ModelE [*Schmidt et al.*, 2006]. From previous model versions improvements have been made in basic physics, stratospheric circulation and forcing fields [*Shindell et al.*, 2001]. The horizontal resolution used here is $4° \times 5°$ latitude by longitude. Since the focus of this study is tropospheric chemistry of trace gases the model atmosphere is configured in 12 vertical layers (Figure 1) with greater resolution in the lower troposphere and the model top at 10 mb to reduce computational time. For present-day simulation 1990 boundary conditions are used for SSTs and sea ice [*Rayner et al.*, 2003], and greenhouse gases. Dynamics, radiation, clouds, land and water surfaces, land ice, sea ice, and surface fluxes are as described by *Schmidt et al.* [2006].

2.2. Chemistry

[7] The GISS tropospheric chemistry model is embedded within ModelE. The model includes a comprehensive suite of reactions for background HO_X-NO_X-O_X-CH_4-CO chemistry (HO_X = OH + HO_2; NO_X = NO + NO_2 + NO_3 + HONO; O_X = O + $O(^1D)$ + O_3) and are described in detail by *Shindell et al.* [2001, 2003]. The chemical family approach is used which allows the chemical time step to be increased to 1 hour and reduces the number of tracers, thus simplifying calculation of chemical changes for some species and decreasing computational time. The model comprises 77 reactions, and accounts for changes in ozone from partitioning within the NO_X family, heterogeneous hydrolysis of N_2O_5 into HNO_3 on sulfate aerosols and phase transformations of soluble species in clouds. Transport within convective plumes, scavenging within and below updrafts, rainout, washout, evaporation of precipitation, and detrainment and evaporation from convective plumes are included [*Koch et al.*, 1999; *Shindell et al.*, 2001]. Since the chemistry is fully interactive with the hydrological cycle it responds to changes in climate through changes in humidity, clouds, precipitation, temperature, and circulation. Dry deposition is calculated using a resistance-in-series method with the vegetation component prescribed. The model fully represents the methane cycle, including detailed emissions, the chemical oxidation pathway, stratospheric loss, and soil absorption.

[8] All simulations were run to steady state equilibrium, run times ranging from 15 to 33 years. The final three years

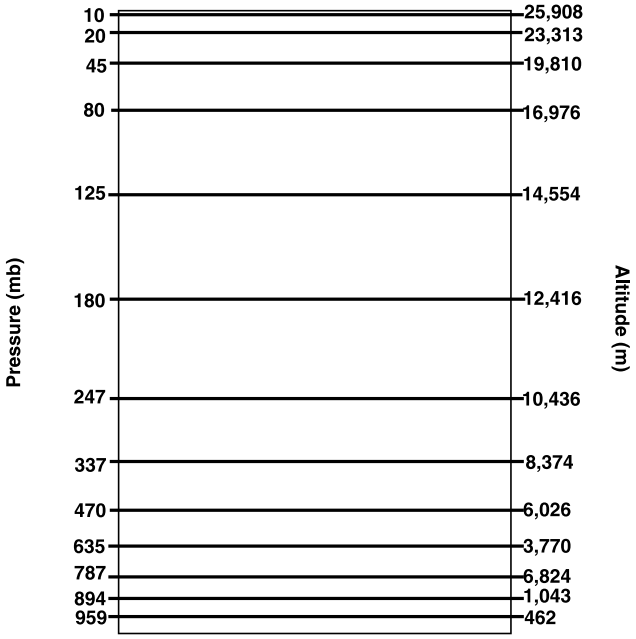

Figure 1. GISS GCM 12-Layer ModelE vertical resolution.

were used to calculate annual average mixing ratios. Interannual variability is negligible, the standard deviation of the 3-year averages being <0.2%. Mixing ratios calculated by the model are for dry air.

2.3. Sources and Sinks

[9] Present-day (PD) CH_4 emissions, listed in Table 1, are based on the work of *Fung et al.* [1991] and *Shindell et al.* [2003]. Briefly, all source fields, excepting wetlands, are scaled according to *Fung et al.* [1991] estimates of individual source strengths and spatial distributions. Wetland emissions are shifted latitudinally toward the tropics in agreement with the meridional distribution adopted by the *World Meteorological Organization* [1999] based on the work of *Whalen and Reeburgh* [1992] and *Bartlett and Harris* [1993], and adjusted in magnitude according to *Hein et al.* [1997], *Houweling et al.* [2000], *Matthews* [2000], and *Walter et al.* [2001]. Emissions are varied seasonally for biomass burning, wetlands and tundra, and rice cultivation. Wetland emissions are 146 Tg/yr and total CH_4 emissions are 529 Tg/yr. Emissions for each category and total emissions are in close agreement with *Prather et al.* [2001] and references therein. The latitudinal distribution of total emissions is shown in Figure 2a. Though recent works of *Frankenberg et al.* [2005] and *Keppler et al.* [2006] suggest that current CH_4 emissions may be greater than previously believed, particularly in the tropics, global emissions inventories based on these findings are uncertain [*Kirschbaum et al.*, 2006]. The CH_4 sink is largely through oxidation by OH, which is calculated in the model, and to a smaller degree by soil absorption which is set to 30 Tg/yr after *Houweling et al.* [2000] (1 Tg/yr, 10 Tg/yr, and 19 Tg/yr occurring in southern, northern, and tropical latitudes, respectively) and stratospheric loss, ~40 Tg/yr globally.

[10] Other trace gas emissions documented by *Shindell et al.* [2003] and include NO_X, CO, isoprene, alkenes, and paraffins. CO sources include biomass burning and industry. NO_X sources include fossil fuel, soil, biomass burning, and aircraft. NO_X is also produced in the model from lightning parameterized using a GISS convection scheme [*Schmidt et al.*, 2006]. Isoprene has a vegetation source, and alkene and paraffin sources include vegetation, industry, and biomass burning.

2.4. Earlier Holocene Model

[11] For these simulations monthly mean SSTs and sea ice were set according to reconstructed values for the decade 1875–1885 [*Rayner et al.*, 2003]. Although earlier (before 1850) SSTs should be slightly cooler the difference is not significant [*Grenfell et al.*, 2001]. Surface vegetation is maintained as in the PD simulation. Because the 12-layer model focuses on tropospheric processes stratospheric constituents are maintained at present day values.

Table 1. Methane Sources in PD and Holocene Base Simulations

	PD				Holocene Base			
Sources, Tg CH_4/yr	Southern Hemisphere 30°S–90°S	Tropics 30°S–30°N	Northern Hemisphere 30°N–90°N	Global	Southern Hemisphere 30°S–90°S	Tropics 30°S–30°N	Northern Hemisphere 30°N–90°N	Global
Animals	9.7	48.0	47.8	105.5	1.7	8.6	8.6	19.0
Coal mine	1.6	4.0	24.6	30.1	0.0	0.0	0.0	0.0
Gas leak	0.7	2.9	33.6	37.2	0.0	0.0	0.0	0.0
Gas venting	0.9	7.3	8.9	17.1	0.0	0.0	0.0	0.0
Municipal solid waste	1.8	8.6	44.9	55.3	0.0	0.0	0.0	0.0
Soil absorption	−1.1	−9.7	−19.3	−30.1	−0.4	−3.7	−7.3	−11.5
Termites	0.7	14.9	4.5	20.1	0.7	14.9	4.5	20.1
Coal combustion	0.2	5.3	10.5	16.1	0.0	0.0	0.0	0.0
Ocean	4.1	6.5	2.9	13.5	4.1	6.5	2.9	13.5
Fresh water lakes	0.1	1.3	3.6	5.0	0.1	1.3	3.6	5.0
Misc. ground[a]	0.4	3.3	3.4	7.0	0.4	3.3	3.4	7.0
Biomass burning	0.0	39.7	0.5	40.2	0.0	4.0	0.0	4.0
Rice cultivation	1.1	45.7	13.4	60.3	0.0	0.0	0.0	0.0
Wetlands and tundra	2.8	74.2	69.1	146.1	3.2	82.5	77.5	163.1
Total	25.8	252.0	251.5	529.4	9.8	117.4	93.1	220.3

[a]Includes volcanoes and hydrothermal vents.

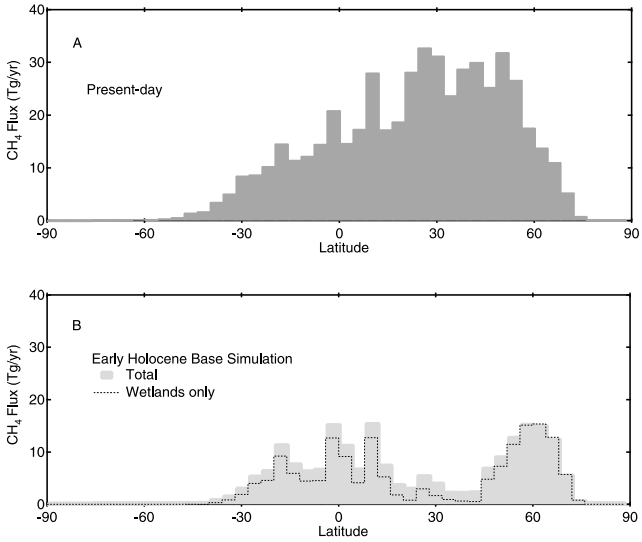

Figure 2. Latitudinal distribution of prescribed methane emissions, (a) present-day and (b) Holocene base simulation.

[12] There is a wide range of estimates for PI Holocene CH_4 emissions calculated using both bottom-up, top-down, and process modeling methods with the global source ranging from 136 to 252 Tg/yr [*Kaplan*, 2002, and references therein; *Valdes et al.*, 2005]. CH_4 emissions used here are listed in Table 1 and produce a global total of 220 Tg/yr. Although 1880 is not truly preindustrial, emissions for this time are used to maintain consistence with the SST and sea ice fields. All anthropogenic emissions are removed. Although emissions from rice cultivation have been estimated from 5 to 15 Tg/yr [*Houweling et al.*, 2000] for the PI Holocene they are not included here. If a best guess of 10 Tg/year were used the total flux would increase only 4% and would not impact our conclusions. Emissions from termites, the ocean, lakes, and miscellaneous ground sources are maintained at PD levels; emissions from animals and biomass burning are reduced to 18% and 10% of PD levels and wetland emissions are set to 163 Tg/yr [*Houweling et al.*, 2000] with the spatial distribution as in the PD simulation. The model CH_4 distribution is dominated by wetland emissions accounting for 83% of total northern emissions and 70% in the tropics (Figure 2b). Because CH_4 emissions were not constant throughout the Holocene, to cover the range of possible changes we ran several simulations altering the magnitude and distribution of wetland emissions from this Holocene base (HB) simulation. These runs are described in detail in section 5.1.

[13] Modifications for other trace gases include removing all anthropogenic emissions, decreasing all biomass burning emissions to 10% of PD, increasing forest emissions of isoprenes, paraffins, and alkenes by 25%, decreasing soil NO_X by 1/3, decreasing N_2O emissions by 12%, and parameterizing CO_2 in agreement with 1880 values [*Shindell et al.*, 2003]. Sulfate aerosols are according to *Koch et al.* [1999]. The soil sink is assumed to be linearly dependent on the atmospheric mixing ratio [*Houweling et al.*, 2000; *Ridgewell et al.*, 1999] and is reduced by 38% from PD. Removal by oxidation and stratospheric mixing are calculated in the model.

2.5. Cold-Climate Model

[14] ModelE simulations were performed using four different prescribed SST and sea ice configurations representative of colder pre-Holocene climates (Table 2). Ice sheet growth is not included in the model, therefore, these simulations cannot be considered to strictly reflect specific climate periods. A Younger-Dryas (YD) representation comprises a tropical annual average SST and annual average lake and ocean ice coverage 0.2°C cooler and 0.9% greater than Holocene [*Rind et al.*, 2001]. The model anomalies are an imposed constraint to a simulation of the coupled models with no North Atlantic Deep Water formation. North Atlantic SST is reduced by ~12°C but global mean and tropical SST change little. Glacial representations based on CLIMAP (CL) and modified CLIMAP (MCL) have sea ice coverage 6.3% greater than Holocene and tropical SSTs 1°C and 2.6°C colder than the Holocene. The coldest glacial representation, based on the work of *Webb et al.* [1997] (WB), has an ice coverage of 7.6% greater than, and a tropical SSTs 6°C colder than, the Holocene. Because the model in these experiments does not include ice sheet growth, change in the northern wetland CH_4 source is approximated by setting emissions within latitudes 30°N to 90°N to 0. All other conditions were as in the Holocene simulation.

3. Present-Day Simulated Atmosphere

3.1. Methane

[15] Simulated annual average surface CH_4 mixing ratio is shown in Figure 3 along with 1990 observations [*Climate Monitoring and Diagnostics Laboratory*, 2005a;

Table 2. Climate Simulations

	Tropical SST (°C)/Reference Sea Ice Coverage, %		Global CH4 Flux, Tg/yr	Global VOC Flux, Tg/yr	Global CO Flux, Tg/yr
PD	25.9/4.2	*Rayner et al.* [2003]	529[a]	580[b]	988[c]
HB	25.5/4.6	*Rayner et al.* [2003]	220[a]	726[b]	49[c]
YD	25.3/5.5	*Rind et al.* [2001]	126[d]	726[b]	49[c]
CL	24.5/10.9	*CLIMAP project members* [1981]	126[d]	726[b]	49[c]
MCL	22.9/10.9	this work	126[d]	726[b]	49[c]
WB	19.5/12.2	*Webb et al.* [1997]	126[d]	726[b]	49[c]

[a]Referenced within text.
[b]*Shindell et al.* [2003]; includes isoprene, paraffins, and alkenes.
[c]*Shindell et al.* [2003]; includes industrial and biomass burning emissions for PD and estimated PI biomass burning emissions for other simulations.
[d]Flux is total HB emissions minus northern (30N–90N) wetland emissions.

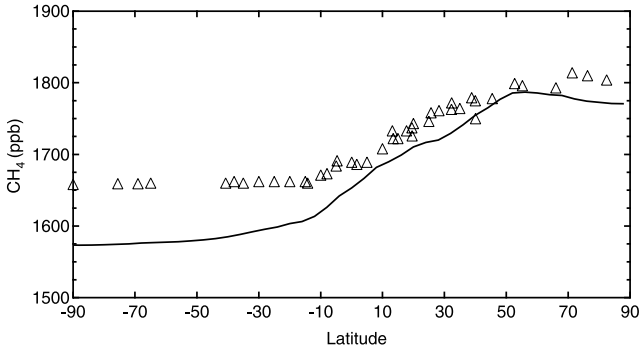

Figure 3. Comparison of 1990 annual average simulated and observed surface CH_4 mixing ratios. The solid line indicates latitudinal averages of simulated values. Triangles indicate surface flask measurements [*Climate Monitoring and Diagnostics Laboratory*, 2005a; *Dlugokencky et al.*, 2005].

Dlugokencky et al., 2005]. Simulated values are generally lower than observations, by as much as 2% in the Northern Hemisphere and by 5% at high southern latitudes. The simulated IPG of 12.3% is, therefore, somewhat larger than the observed value of ~9%. By focusing on the sensitivities of the CH_4 mixing ratio and gradient we minimize the effects of these errors in absolute magnitude as shown in section 5.2. The simulated global mean CH_4 life time, 10.1 years, is somewhat larger than the observed value of 8.4 years used by *Intergovernmental Panel on Climate Change* [2001] (hereafter IPCC, 2001) from the work of *Prather et al.* [1995] and *Schimel et al.* [1996], suggesting that OH is to some extent depleted. The life time based solely on removal by OH is 12.3 years, again larger than the IPCC value of 9.6 years estimated from a methylchloroform derived OH lifetime [*Prather et al.*, 2001; *Prinn et al.*, 1995; *Spivakovsky et al.*, 2000]. The simulated value is sensitive to emissions of CO and hydrocarbons, ozone photolysis rates, humidity and circulation, thus biases may be reflective of the uncertainties in any of these factors.

3.2. Carbon Monoxide

[16] Model results for carbon monoxide (CO) are compared with observations [*Climate Monitoring and Diagnostics Laboratory*, 2005b; *Novelli et al.*, 1998] in Figure 4. Simulated zonally averaged mixing ratio is generally greater than measurements, in the Southern Hemisphere by 30–40% and in the Northern Hemisphere by 35–40% in mid and high latitudes. The IPG is well represented, the simulated and observed values being 215% and 210%, respectively. Simulated and observed annual cycles for specific sites are compared in Figure 5. The model reproduces the annual cycles well but again the mixing ratios are, on average, 30% higher than observations.

[17] Some of the difference between measured and modeled values for CO is likely due to the grid box size in the model. Sampling sites are commonly in remote unpolluted locations, while the large model boxes may include emissions from relatively distant sources that do not affect the measurements, especially as these are screened to remove "pollution events". Probably of more importance, the larger prescribed VOC emissions may also contribute to the high simulated CO, as isoprene forms CO when oxidized. The general overestimate of CO is consistent with the high CH_4 lifetime, and again it suggests that while the uncertainty is large, VOC emissions may be set slightly high, and/or CH_4 emissions set low, for this model. We also note that simulated CO is sensitive to OH which is in turn a function of the model's hydrologic cycle. A similar ModelE Holocene simulation using greater vertical resolution produces more realistic OH and CO with almost identical emissions [*Shindell et al.*, 2005].

4. Premodern Holocene Atmosphere

[18] Opportunities to test the accuracy of the premodern Holocene simulations are limited. Although PI surface ozone has been reconstructed, preindustrial surface ozone measurements are limited spatially and temporally so that tropospheric ozone abundance, distribution, and trends are not well known [*Pavelin et al.*, 1999; *Shindell and Faluvegi*, 2002]. Thus we do not make simulated and observational ozone comparisons here. The most accurate observations for preindustrial trace gases are from ice core records. Observational comparison for Holocene simulations is, therefore, restricted to CH_4 and CO.

4.1. Methane

[19] Surface CH_4 mixing ratio for the HB simulation (Figure 6) agrees well with ice core observations [*Etheridge et al.*, 1998] in high northern latitudes for the 1870's but is 9% lower in high southern latitudes. The resulting IPG, 14.3%, is almost 3 times greater than the value of 5.2% ± 0.64% calculated from observations. Figure 6 also shows a comparison for an earlier Holocene period (250–1000 yr B.P.) from *Chappellaz et al.* [1997]. The dashed line represents a simulation in which CH_4 emissions have been decreased 50% from the HB simulation in the extra-tropical north. Here the mixing ratios are again smaller than observations, 6% and 9% for high northern and southern latitudes, respectively. The simulated IPG, 8.7%, is still greater than that calculated observations, 5.2%, but is closer than for the comparison with the HB simulation. Though these

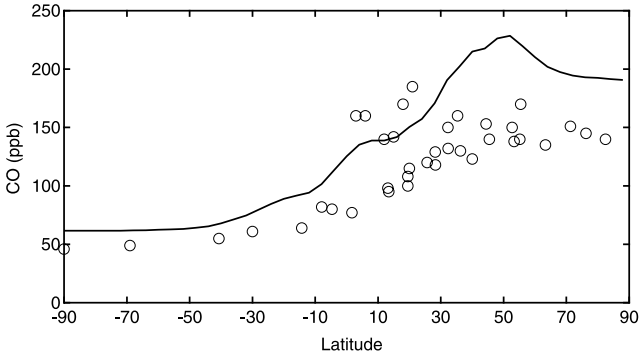

Figure 4. Comparison of 1990 annual average simulated and observed surface CO mixing ratio. The solid line indicates latitudinal averages of simulated values. Circles indicate measurements (*Climate Monitoring and Diagnostics Laboratory*, 2005b; *Novelli et al.*, 1998].

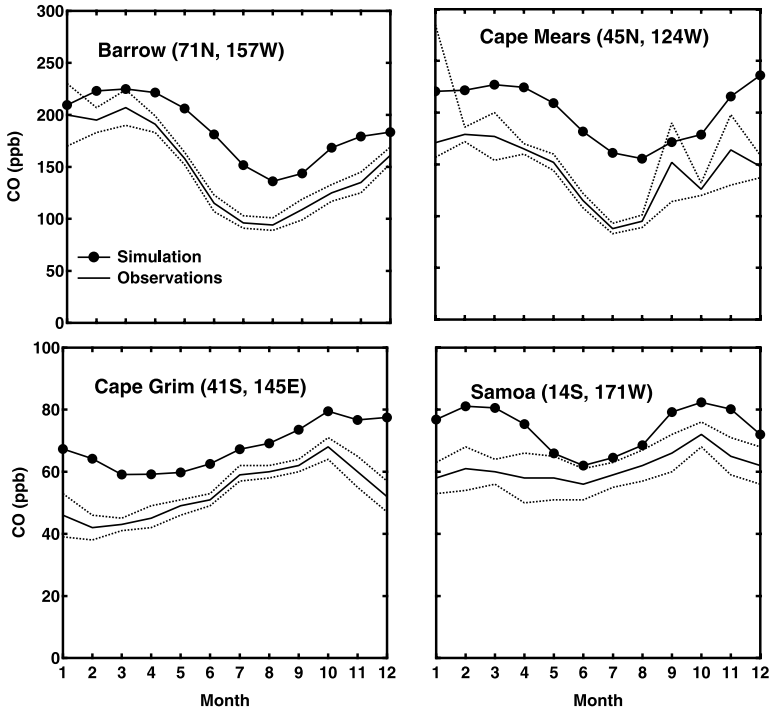

Figure 5. Comparison of 1990 simulated and observed monthly mean surface CO mixing ratio. Solid lines indicate measured values and dotted lines are standard deviations [*Novelli et al.*, 1998]. Solid circles indicate simulated values.

comparisons are not ideal, they characterize the sensitivity of the CH_4 mixing ratio and IPG in a space that either spans or is quite near observed values. As we analyze numerous simulations to obtain a broad view of these sensitivities, the precise values produced by any given simulation are less important. We can in fact estimate the sensitivity relative to any reasonably proximate initial state, with errors arising only from potential incomplete characterization of the small nonlinearity in the CH_4 response (section 5.2). Given the large uncertainties in trace gas emissions within the Holocene, the differences between the model and observations do not necessarily indicate a flaw in the chemistry simulation. Simulated global mean atmospheric lifetime for CH_4 has increased from the PD by 16% to 11.7 years. Results from other models range from a decrease of 17% to an increase of 16% [*Martinerie et al.*, 1995; *Berntsen et al.*, 1997; *Brasseur et al.*, 1998; *Mickley et al.*, 1999; *Shindell et al.*, 2003]. Again, the wide range of results for the difference in the CH_4 sink from PD to earlier Holocene are consistent with the poor constraints on PI trace gas emissions since OH abundance, and the resulting CH_4 lifetime, are determined by a complex set of interactive chemical reactions, notably the CH_4 feed back on its own lifetime and the opposing influence of NO_X.

4.2. Carbon Monoxide

[20] Simulated Holocene surface CO mixing ratio (Figure 7) shows a more symmetrical distribution than for the PD because the industrial source, located primarily in midnorthern latitudes, is removed. The distribution is primarily a function of the biomass burning flux which is

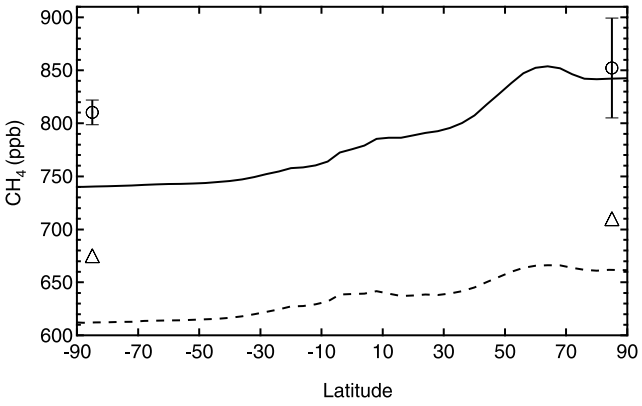

Figure 6. Comparison of simulated Holocene simulations and ice core CH_4. The solid line represents latitudinally averaged simulated mixing ratios for the HB simulation. Open circles represent average values from ice core measurements of *Etheridge et al.* [1998] from Law Dome, Antarctica and Summit, Greenland. The Antarctic data point and error bars are the mean and standard deviation for 3 measurements dating from 1863 to 1879. The Greenland data point and error bars are the mean and standard deviation for 2 measurements dated 1842 and 1885. The dashed line shows CH_4 mixing ratio for the N-50 simulation. Triangles are averages for the RH period from ice core data [*Chappellaz et al.*, 1997]. The standard deviations for these two points fall within the symbols and are 2% and 6% for Greenland and Antarctica, respectively.

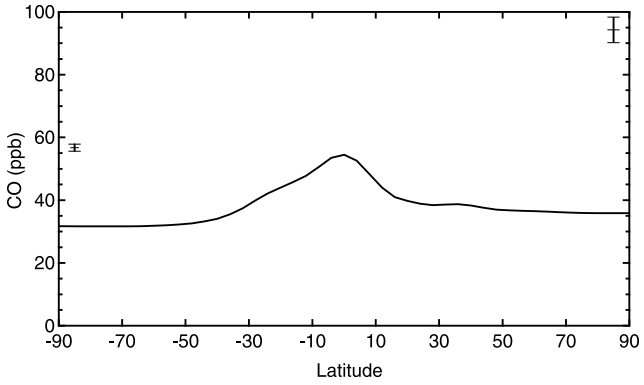

Figure 7. Comparison of simulated Holocene base simulation and ice core CO. The solid line represents latitudinally averaged simulated values. Bars represent average values from ice core measurements of *Haan et al.* [1996] from Vostok, Antarctica and Summit, Greenland. The Antarctic data point and error bar are the mean and standard deviation for six measurements dating from 1860 to 1916. The Greenland data point and error bar are the mean and standard deviation for nine measurements dated from 1802 to 1905.

centered in the tropics. The simulated mixing ratio at high latitudes is 44% and 62% lower in the south and north, respectively, than ice cores observations of *Haan et al.* [1996]. The observed values shown in Figure 7 are means for the period ranging from 1860 to 1916 for Antarctic measurements and from 1802 to 1905 for Greenland measurements. The simulated IPG is 13% compared to 62% from ice core data. This difference is may result directly from CO emissions and indirectly through CO production by CH_4 and VOC oxidation, all of which may be low. CO may also be produced photochemically from carbonyl compounds in fresh snow, firn, and ice [*Haan et al.*, 2001], so that mixing ratios measured in ice cores may be elevated from original atmospheric levels, although the consistency of the measurements for the period surrounding the mid 1800's argues against this potential bias. More recent Antarctic ice core measurements [*Ferretti et al.*, 2005] found CO ranging from 50 to 90 ppb in Antarctica for the period 0 to 1600 AD further indicating that simulated CO is somewhat low.

5. Earlier Holocene Methane

5.1. Sensitivity Experiments

[21] Experiments were conducted varying the amount and distribution of wetland CH_4 emissions from the HB simulation (Table 3). From the base, wetland CH_4 emissions were globally adjusted by −50% and +50%. Tropical wetland emissions were adjusted by +50%, −50%, −75%, and −90%, northern wetland emissions were adjusted by +50%, −50%, and −100%, and northern and southern emissions together were adjusted by −100%. Experiments were also conducted for VOC emissions. Maintaining the global distribution, emissions were reduced by 50%, 75%, and 90%.

[22] For each experiment the IPG is calculated for the 4° latitude bands encompassing most Greenland and Antarctic ice core sites, 72°N to 76°N and −80°S to −76°S, to allow comparison with IPGs calculated from ice core data. Calculated lifetimes, τ, include removal by OH, soil absorption, and stratospheric loss.

Table 3. GCM Sensitivity Experiments

Experiment	Wetland CH_4 Emissions[a]
PD	present-day emissions
HB	Holocene base emissions
G−50	HB: Global CH_4 emissions decreased 50%
G+50	HB: Global CH_4 emissions increased 50%
T+50	HB: Tropical CH_4 emissions increased 50%
T−50	HB: Tropical CH_4 emissions decreased 50%
T−75	HB: Tropical CH_4 emissions decreased 75%
T−90	HB: Tropical CH_4 emissions decreased 90%
N+ 50	HB: Northern CH_4 emissions increased 50%
N−50	HB: Northern CH_4 emissions decreased 50%
N−100	HB: Northern CH_4 emissions decreased 100%
NS−100	HB: Northern and Southern CH_4 emissions decreased 100%
VOC−50	HB: Global VOC emissions decreased 50%
VOC−75	HB: Global VOC emissions decreased 75%
VOC−90	HB: Global VOC emissions decreased 90%
YD	N−100 CH_4 emissions
CL	N−100 CH_4 emissions
MCL	N−100 CH_4 emissions
WB	N−100 CH_4 emissions
WB/HB	HB emissions

[a]Tropical encompasses the region within latitudes 30°S–30°N. Northern encompasses the region within latitudes 30°N–90°N. Southern encompasses the region within latitudes 30°S–90°S.

5.2. Results

[23] Qualitatively CH_4 mixing ratio and IPG change as expected depending on the perturbation in each experiment (Table 4). Mixing ratio decreases with decreasing CH_4 emissions and increases with increasing CH_4 emissions.

Table 4. Current-Day, Preindustrial, and Sensitivity Study CH_4 Results

Experiment	CH_4 Conc. Global, ppb	CH_4 Conc. Greenland, ppb	CH_4 Conc. Antarctica, ppb	IPG, %	τ Global, years
PD	1661	1778	1574	12.3	10.1
HB	778	846	741	14.3	11.7
Sensitivity Studies					
G−50	472	507	452	12.2	10.5
G+50	1127	1227	1073	14.3	12.7
T+50	920	979	877	11.6	12.2
T−50	629	701	593	18.3	11.2
T−75	544	622	509	22.2	10.8
T−90	500	577	465	24.1	10.7
N+ 50	941	1046	886	18.0	12.3
N−50	632	666	612	8.7	11.2
N−100	473	464	468	−0.7	10.5
NS−100	469	460	463	−0.6	10.5
VOC−50	719	786	682	15.3	10.3
VOC−75	681	750	645	16.3	9.7
VOC−90	665	736	628	17.1	9.4
Glacial Simulations					
YD	488	480	483	−0.5	10.7
CL	497	489	490	−0.1	11.3
MCL	584	575	576	−0.3	13.0
WB	727	717	719	−0.2	16.5
WB/HB	1175	1237	1134	9.0	18.2

IPG becomes larger with increasing northern wetland emissions and decreasing tropical emissions, and becomes smaller with opposite shifts in emissions distribution. As VOC emissions decline CH_4 mixing ratio decreases and IPG increases. This response is the result of a larger OH sink arising from the decline in VOCs which compete with CH_4 for oxidation. The IPG response results from the largely equatorial distribution of VOC emissions. The impact on CH_4 mixing ratio is much greater in the tropics than in the north and drives the change in the IPG.

[24] Figure 8 shows contour plots derived from the results of the Holocene sensitivity experiments. Experiment N-50 is used as the base simulation to calculate Holocene sensitivities because it provides the best match for the most recent Holocene period (250–1000 yr B.P.) for which *Chappellaz et al.* [1997] calculated mixing ratios and IPG from ice core data. Polynomials have been fitted to the sensitivities for northern and tropical emissions changes. The contours describe the difference from the N-50 for CH_4 mixing ratio and IPG as a function of per cent change in tropical and northern emissions. The response of both mixing ratio and IPG to changes in tropical and northern flux are not linear (Figures 8a and 8b). Mixing ratio sensitivity increases with increasing northern emissions, IPG becomes more sensitive as tropical emissions decrease. This nonlinearity is not surprising considering the complexity and interdependence of oxidation chemistry, differences in northern, tropical, and southern CH_4 lifetimes, and atmospheric dynamics.

[25] For a specific time period the change in CH_4 mixing ratio and IPG calculated from ice core data can be used together to constrain the percentage change in northern and tropical CH_4 emissions as demonstrated by Figure 8c, which overlays the two preceding plots. The changes in northern and tropical emissions are found at the point of intersection of the specified mixing ratio and IPG contour lines. We use this method to determine the change from the recent Holocene in the emissions distribution for selected periods in the earlier Holocene.

[26] *Chappellaz et al.* [1997] calculated average CH_4 mixing ratios from Greenland and Antarctic ice core data for four Holocene time periods (Table 5): Recent Holocene (RH, 250–1000 yr. B.P.), mid-Holocene (MH1, 2500–5000 yr. B.P.), early mid-Holocene (MH2, 5000–7000 yr. B.P.), and Preboreal (PB, 9500–11,500 yr. B.P.). Taking MH1 as an example, the change in mixing ratio and IPG are 100 ppb and 3.6%. The point of intersection of these two contours is marked with a cross in Figure 8c. Dashed arrows indicate the corresponding changes, on the X and Y axes, in northern and tropical emissions required by the simulation to produce the observed IPG and mixing ratio. Points of intersection for MH2 and PB are also shown. Emission changes for the three Holocene periods obtained in this manner are shown as gray bars in Figure 9. During PB topical CH_4 emissions were slightly lower than during RH. As CH_4 mixing ratio declined during MH1 and MH2,

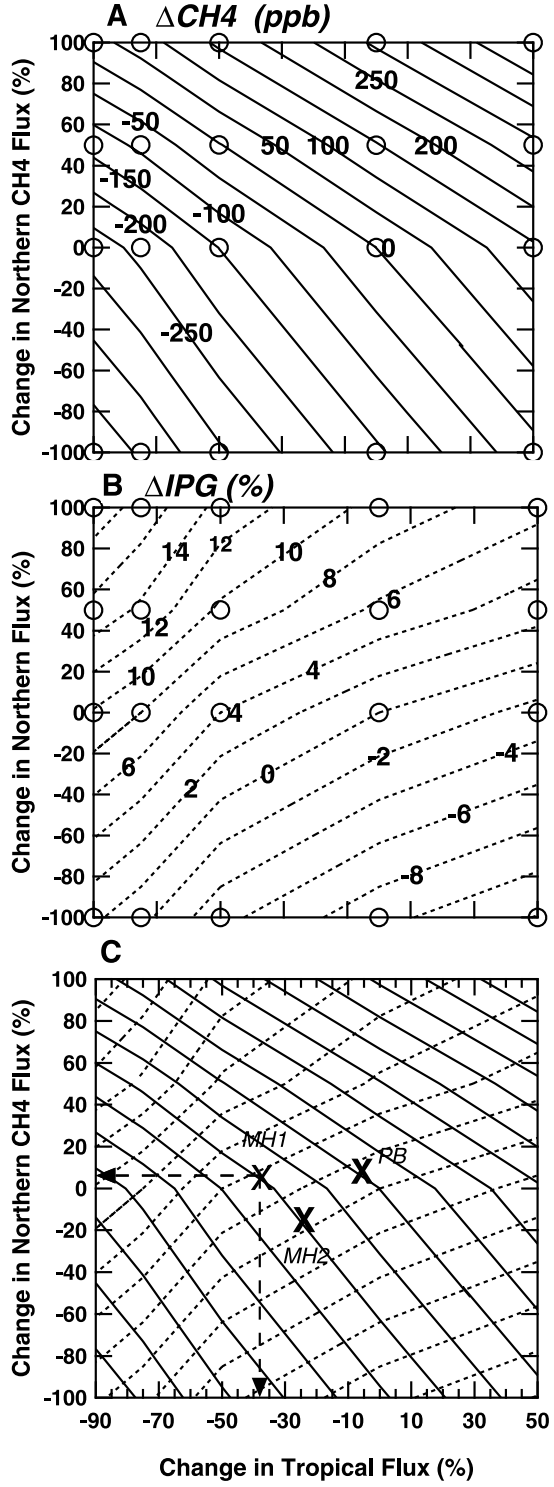

Figure 8. Sensitivity of the change from the RH for (a) CH_4 mixing ratio (contours are in increments of 50 ppb) and (b) IPG (contours are in increments of 2%) as a function of the percent change in tropical and northern CH_4 flux. Circles are calculated points used in the interpolation of the contours. (c) Mixing ratio and IPG contours are overlaid. Large crosses show the intersection of the two contour lines for specific periods derived from ice core data. Dashed arrows show corresponding percent change in tropical and northern CH_4 flux for the period MH1.

Table 5. CH_4 Mixing Ratios and IPGs for Specific Holocene Periods From *Chappellaz et al.* [1997]

	RH	MH1	MH2	PB
Greenland conc, ppb	710	617	608	718
Antarctic conc., ppb	675	567	575	674
Global mean conc., ppb	692.5	592.0	591.5	696.0
ΔConc. from RH, ppb		−101.0	−100.5	3.5
IPG, %	5.2	8.8	5.7	6.5
ΔIPG from RH, %		3.6	0.5	1.3

tropical emissions decreased by 38% and 25%, respectively, compared to RH. Northern emissions were more stable throughout the Holocene, increasing by 6% and 8% from RH in MH1 and PB, respectively, and decreasing by 15% during MH2. The black bars in Figure 9 show the results of the three-box model [*Chappellaz et al.*, 1997] for comparison. The change in tropical emissions is negative and of similar size as the GCM results. However, for northern emissions, while the sign of the change is the same for the two models, the degree of change differs appreciably. This difference increases as the tropical source becomes smaller, so that for MH1, with a decrease in tropical emissions of 38%, the box model produces northern emissions that are almost 4 times greater than those estimated by the GCM. This result is not surprising in light of the nonlinear response of the simulated sensitivities (Figure 8). The simpler box model is based on the mass balance of CH_4 assuming a constant sink and a linear relationship between box mixing ratios and the northern and tropical source at steady state and, therefore, overestimates northern CH_4 flux for situations in which the change in the tropical flux is large.

[27] To test the sensitivity of this method to the absolute magnitude of simulated mixing ratios and gradient used as the starting point for contour construction we also performed this analysis using the HB simulation as the base for calculating the contour plots of Figure 8. The resulting differences in stipulated northern and tropical flux changes for each Holocene period range from only 1–4%, so that within the mixing ratio and IPG limits of this study the model sensitivity does not greatly change. The two base simulations used, HB and N-50, bracket the RH ice core mixing ratios; therefore a 4% change in emissions can be considered the upper limit for uncertainty in the results owing to observation/simulation differences in absolute mixing ratios. Simulated IPGs do not bracket ice core results and therefore the uncertainty is not strictly constrained. However, if we assume that the entire 4% change in emissions arises from the change in IPG from the HB to the N-50 simulation (Table 4, change in IPG = 5.6%) and extrapolate to the change in IPG from N-50 to the observed RH IPG (Table 5, change in IPG = 3.5%) we increase the uncertainty by 2.5% making the maximum uncertainty in estimated Holocene emissions 6.5%. The true uncertainty is probably lower since inaccuracy in the mixing ratio must contribute to some degree.

[28] During the Holocene changes in atmospheric OH from changing VOC emissions may also need to be considered. *Adams et al.* [2000] suggest that VOCs increased by as much as 20% with a concomitant decrease in the OH sink. Although sensitivity studies were performed only for decreasing VOC emissions, results indicate a fairly linear response for CH_4 mixing ratio. Extrapolation to a 20% increase shifts mixing ratio and IPG contour lines in Figure 8 by about +26 ppb −0.6%, respectively. The changes in CH_4 emissions for MH1 and MH2, shown as dashed lines in Figure 9, decrease an additional 8% in the tropics and by 2% in the north. These results are as expected. Rising VOCs reduce atmospheric oxidation capacity and increase CH_4 lifetime, so that to maintain a given CH_4 mixing ratio fewer CH_4 emissions are required. To maintain a given IPG, since VOC emissions are primarily tropical in origin, the decline in CH_4 emissions must be greater in the tropics than in the north.

6. Cold-Climate Methane

[29] During glacial-interglacial transitions the CH_4 source and sink were subject to greater changes in climate than during the Holocene. Northern emissions were also influenced by the degree of ice sheet coverage which impacted boreal wetland extent. Significant decreases in VOC emissions may have played a roll in decreasing CH_4 mixing ratio in the tropics. *Adams et al.* [2000] found a 57% decrease in global Holocene VOC emissions for an LGM vegetation distribution using a 5°C drop in tropical surface temperature. *Valdes et al.* [2005] found a much greater sensi-

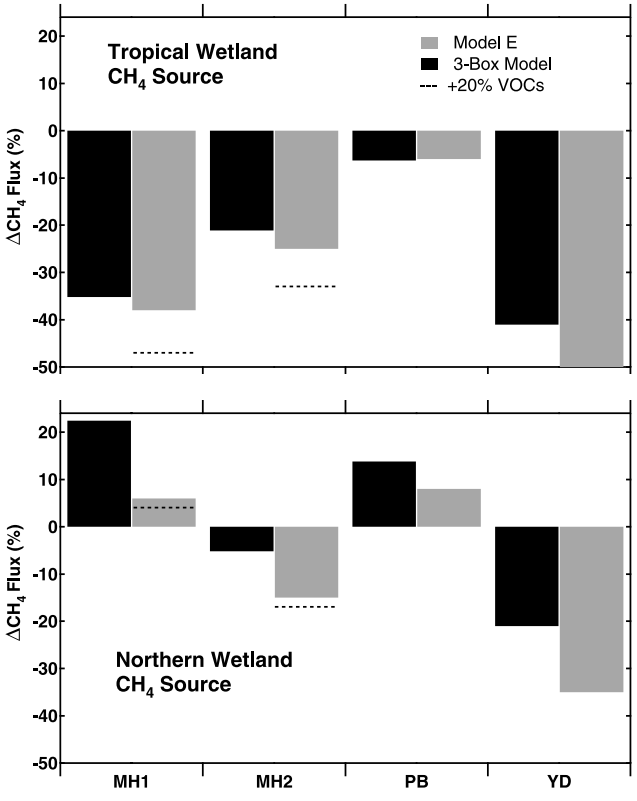

Figure 9. Change in tropical and northern CH_4 flux from the RH for GCM simulations and three-box model results for specific periods. Light bars represent GCM results, dark bars represent box model results, and dashed lines indicate the change in the GCM result if VOC emissions are increased 20%.

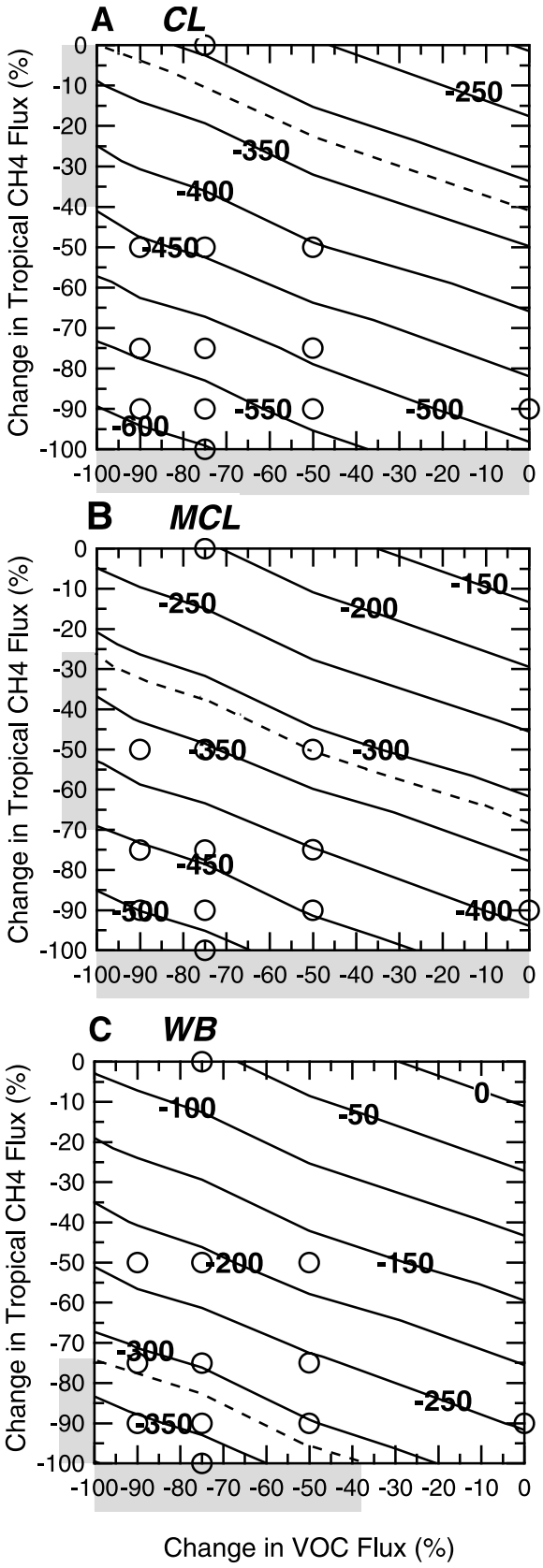

tivity for VOC emissions to LGM climate using a dynamic vegetation model coupled to a GCM with a CLIMAP [*CLIMAP project members*, 1981] climatology which stipulates an average tropical SST cooling of ~1°C. Their results suggest that changes in VOC emissions, through their influence on OH abundance, may have played a large role in changing methane lifetime and mixing ratio. They found that global methane emissions declined 23% from Holocene levels during the LGM, most of the change occurring in the north, tropical emissions decreasing only 3%. Concurrently their simulated VOC emissions, located largely in the tropics, decreased by 50% resulting in a decrease in CH_4 lifetime of 16%. CLIMAP [*CLIMAP project members*, 1981], however, may underestimate cooling at the LGM particularly in the tropics [*Rind and Peteet*, 1985; *Broecker*, 1985; *Webb et al.*, 1997; *Kucera et al.*, 2005]. Since wetland CH_4 emissions, CH_4 oxidation rate, and vegetation VOC emissions all appear to show significant sensitivity to temperature [*Kaplan*, 2002; *Johnson et al.*, 2001; *Adams et al.*, 2000], the questions arise: What is the sensitivity of CH_4 mixing ratio to changes in VOC emissions? How does a cooler LGM climatology impact the change in CH_4 mixing ratio observed between the early Holocene and the LGM?

[30] Experiment N-100 and the cold-climate experiments maintain constant CH_4 and VOC emissions for progressively cooler climates (Tables 2 and 3). They show the expected result that CH_4 lifetime and mixing ratio increase as temperature cools, arising from a decrease in evaporation, atmospheric water vapor, and ultimately OH production with a concomitant slowing of CH_4 oxidation rate (Table 4). Increases in CH_4 mixing ratio of 15, 23, 111, and 254 ppb are found for YD, CL, MCL, and WB simulations, respectively. In removing the northern wetland source the IPG is constrained to be near 0% in these experiments, close to the value of −1% calculated by *Dällenbach et al.* [2000] for the LGM. Experiment NS-100 removes the southern wetland source as well as the northern. The resulting mixing ratio and IPG are the same as for N-100 confirming that changes in southern emissions do not play a large role in determining CH_4 mixing ratio or IPG. The consistent IPG found for these experiments with no northern wetland emissions indicates that the distribution of the sink does not significantly change when emissions are primarily tropical in origin.

[31] The sensitivity of CH_4 mixing ratio to changes in climate, VOC emissions, and tropical CH_4 emissions is shown in the contour plots of Figure 10. Three plots are shown, representing the cold climate experiments CL,

Figure 10. Sensitivity of the change in CH_4 mixing ratio (ppb) from RH to LGM as a function of the percent change in tropical CH_4 and global VOC emissions. Circles are calculated points used in the interpolation of the contours. The dashed lines are the −320 ppb change from RH in global average mixing ratio. Shaded regions of the X and Y axes indicate the range in source change corresponding to the −320 ppb contour. Figures 10a, 10b, and 10c show increasingly colder representations. Contours are in increments of 50 ppb.

MCL, and WB. The contours represent the change in mixing ratio from the Holocene to glacial, calculated using the ice core value for the period RH (Table 5) for the Holocene reference point. If we instead used a simulated Holocene (e.g., HB) mixing ratio as the reference point, the contours shown in Figure 10 would be displaced by about −75 ppb. Thus the observed reference point constrains the emissions changes less tightly than would the modeled value, but is probably more realistic. The simulated difference is the sum of the mixing ratio changes due to climate change and loss of northern wetland source (experiment N-100), varying as a function of changing VOC and tropical CH_4 emissions. Because the IPG is essentially fixed we cannot constrain emissions for this case as closely as for the Holocene. However, with knowledge of the Holocene-LGM mixing ratio difference from ice core data we can more broadly constrain changes in VOC and tropical CH_4 fluxes using Figure 10. Using a value of 693 ppb for the global average Holocene CH_4 mixing ratio [*Chappellaz et al.*, 1997] and ∼375 ppb for the LGM [*Brook et al.*, 2000; *Dällenbach et al.*, 2000], a global average decrease of ∼320 ppb is calculated. Recall that a drop in VOC emissions decreases CH_4 lifetime thereby requiring a larger CH_4 flux to maintain a given atmospheric reservoir. The shaded regions of the axes in Figure 10 highlight the range of possible VOC and tropical CH_4 emissions corresponding to the −320 ppb contour line. Note that a given change in mixing ratio may be attained by changing CH_4 emissions alone, VOC emissions alone, or a combination of the two. As the climate cools, larger decreases in CH_4 and/or VOC fluxes are required to arrive at the specified decrease in mixing ratio. For the warmest glacial representation, CL, the −320 ppb contour falls within the range of a 0% to 100% decrease in VOC flux, and allows for a maximum decrease in tropical CH_4 flux of 40% in the absence of VOC emissions and approaches 0% as VOC flux increases. Here the 50% decline in VOC flux of *Valdes et al.* [2005] requires a 20% decrease in tropical CH_4 emissions. With no change in VOC flux, the tropical CH_4 emissions decrease, 40%, is very close to that calculated from the three-box model [*Dällenbach et al.*, 2000; *Brook et al.*, 2000], analogous to tropical results for the Holocene. Moving toward colder climates, MCL and WB, a 50% decrease in VOC flux would require a 50% and 95% decrease, respectively, in tropical CH_4 flux. To summarize, in comparison with the results of *Valdes et al.* [2005], our warmest glacial experiment, CL, allows for a 3% percent change in tropical CH_4 flux but only for a much larger decrease in VOC flux. The two colder climates allow a decrease of 50% in VOC flux but the changes in tropical flux must be larger. Thus while a 50% reduction in VOC emissions for a CLIMAP LGM is consistent with our results, a smaller drop in VOC emissions, in line with the climate sensitivity reported by *Adams et al.* [2000], could have occurred in conjunction with a significant drop in tropical CH_4 emissions. However, if the LGM climate was as cold as the WB reconstruction indicates, then a large decrease in both tropical CH_4 and VOC emissions would have been necessary to achieve the decline in CH_4 mixing ratio. Though the results are consistent with reductions in VOC emissions, only in the coldest climate are they necessary to account for the observed mixing ratio decrease.

[32] Although the YD representation contains colder SSTs and greater sea ice extent than the Holocene, the Younger-Dryas cannot be considered strictly glacial since ice sheets had retreated appreciably from LGM extent [*Peltier*, 1994], and northern boreal wetland emissions may have increased to some degree [*Dällenbach et al.*, 2000]. Although VOC emissions likely also changed during this period no information is available regarding the direction or magnitude of the change. If constant VOC emissions are assumed we can obtain a first-order estimate of the change in CH_4 flux distribution for the Younger-Dryas from ice core data and Figure 8. From experiments N-100 and YD (Table 4) the change in CH_4 mixing ratio due to YD temperature change is +15 ppb so mixing ratio contours shift by 15 ppb. Although we see from experiment WB/RH that the IPG decreases as climate cools, because the sensitivity of the IPG to changes in emissions is not linear we cannot extrapolate from WB/RH to the YD representation. Assuming the sensitivity of the IPG is not greatly different from the Holocene we can use the IPG contours from Figure 8. Using a change from RH mixing ratio of −221 ppb and IPG of +0.5% for the Younger-Dryas [*Chappellaz et al.*, 1997; *Dällenbach et al.*, 2000], the corresponding changes in CH_4 emissions, shown in Figure 9, are −35% in the north and −50% in the tropics, 14% and 9% lower, respectively, than the estimates of the three-box model. This result is an upper limit for northern emissions and a lower limit for tropical emissions since a shift in IPG contours would result in a greater decline in northern emissions and a smaller decline in tropical emissions. The dependence of estimated CH_4 emissions on ice sheets and VOC emissions, and IPG on climate makes a period such as the Younger-Dryas difficult to evaluate with our current suite of sensitivity studies. A more accurate assessment will require further analysis.

7. Discussion and Conclusions

[33] We have demonstrated a method that combines the ice core CH_4 record with a coupled GCM/atmospheric chemistry model to constrain changes in northern and tropical CH_4 emissions, and VOC emissions for specific climate periods. For the Holocene, using changes in ice core IPG and mixing ratio together can very tightly constrain estimates of CH_4 emissions. Estimates for glacial periods with larger, though less well defined, impacts from climate change are less tightly constrained. Caution must be used in interpreting the ice core CH_4 record as a proxy for changes in wetland CH_4 emissions. Methane mixing ratio shows significant sensitivity to changes in the OH sink when climate change is great enough to substantially influence atmospheric OH production and removal.

[34] Many components of the CH_4 cycle are not comprehensively characterized for the preindustrial Holocene and glacial period. Greater knowledge of changes in ice sheet coverage and topography, and wetland distribution and production are necessary to more accurately determine the CH_4 source for different climate periods. Changes in sea ice, SST, and vegetation VOC emissions must be better defined

to improve representation of the CH_4 sink. Better understanding of other boundary conditions, such as, emissions of the other greenhouse gases, sulfur dioxide, and coarse-mode aerosol will serve to clarify the energy budget and the atmospheric oxidation capacity. Further observational and modeling studies are necessary to achieve these goals.

[35] The method demonstrated here to can also be improved through development of the GISS model. Future work will involve incorporating dynamic wetlands and wetland CH_4 production and interactive vegetation VOC emissions, and tuning model emissions to more accurately represent the observed PD and Holocene CH_4 distributions. Improving specific cold climate parameters; such as, ice sheets and postglacial lakes, soil absorption of CH_4, sulfur dioxide and sulfate aerosol, dust aerosol, and soil NO_x emissions will also improve the accuracy of the analysis.

[36] **Acknowledgments.** The authors thank Greg Faluvegi for programming and data analysis assistance and Nadine Bell for helpful discussion and comments. This work was funded by NASA Summer Faculty Fellowship Program, NASA Summer High School Apprenticeship Research Program, and NOAA Climate and Global Change Fellowship Program.

References

Adams, J. M., J. V. H. Constable, A. B. Guenther, and P. Zimmer (2000), An estimate of natural volatile organic compound emissions from vegetation since the last glacial maximum, *Chemos. Global Clim. Change*, *3*, 73–91.

Bartlett, K. B., and R. C. Harris (1993), Review and assessment of methane emissions from wetlands, *Chemosphere*, *26*, 261–320.

Berntsen, T. K., I. S. Isaksen, G. Myhre, J. S. Fuglestvedt, R. Stordal, T. A. Larsen, R. S. Freckleton, and K. P. Shine (1997), Effects of anthropogenic emissions on tropospheric ozone and its radiative forcing, *J. Geophys. Res.*, *102*, 28,101–28,126.

Brasseur, G. P., J. T. Kiehl, J. F. Muller, T. Schneider, C. Granier, X. Tie, and D. Hauglustaine (1998), Past and future changes in global tropospheric ozone: Impact on radiative forcing, *Geophys. Res. Lett.*, *25*, 3807–3810.

Broecker, W. S. (1985), Cooling in the tropics, *Nature*, *376*, 212–213.

Brook, E. J., T. Sowers, and J. Orchardo (1996), Rapid variations in atmospheric methane concentration during the past 110,000 years, *Science*, *273*, 1087–1091.

Brook, E. J., S. Harder, J. Severinghaus, E. J. Steig, and C. M. Sucher (2000), On the origin and timing of rapid changes in atmospheric methane during the last glacial period, *Global Biogeochem. Cycles*, *14*, 559–572.

Chappellaz, J., J. M. Barnola, D. Raynaud, Y. S. Korotkevich, and C. Lorius (1990), Ice-core record of atmospheric methane over the past 160,000 years, *Nature*, *345*, 127–131.

Chappellaz, J., I. Y. Fung, and A. M. Thompson (1993), The atmospheric CH_4 increase since the Last Glacial Maximum, *Tellus, Ser. B*, *45*, 228–241.

Chappellaz, J., T. Blunier, S. Kints, A. Dallenbach, J. M. Barnola, J. Schwander, D. Raynaud, and B. Stauffer (1997), Changes in the atmospheric CH_4 gradient between Greenland and Antarctica during the Holocene, *J. Geophys. Res.*, *102*, 15,987–15,997.

CLIMAP project members (1981), Seasonal reconstructions of the Earth's surface at the Glacial Maximum, *Map Chart Ser. 36*, Geol. Soc. of Am., Boulder, Colo.

Climate Monitoring and Diagnostics Laboratory (2005a), GLOBALVIEW-CH4: Cooperative Atmospheric Data Integration Project—Methane [CD-ROM], Boulder, Colo. (Available via anonymous FTP to ftp.cmdl.noaa.gov, Path: ccg/ch4/GLOBALVIEW)

Climate Monitoring and Diagnostics Laboratory (2005b), GLOBALVIEW-CO: Cooperative Atmospheric Data Integration Project—Carbon monoxide [CD-ROM], Boulder, Colo. (Available via anonymous FTP to ftp.cmdl.noaa.gov, Path: ccg/co/GLOBALVIEW)

Crowley, T. J. (1995), Ice age terrestrial carbon changes revisited, *Global Biogeochem. Cycles*, *9*, 377–390.

Crutzen, P. J., and C. Brühl (1993), A model study of atmospheric temperatures and the concentrations of ozone, hydroxyl, and some other photochemically active gases during the glacial, the preindustrial Holocene and the present, *Geophys. Res. Lett.*, *20*, 1047–1050.

Dällenbach, A., T. Blunier, J. Fluckinger, and B. Stauffer (2000), Changes in the atmospheric CH_4 gradient between Greenland and Antarctica during the Last Glacial and the transition to the Holocene, *Geophys. Res. Lett.*, *27*, 1005–1008.

Dlugokencky, E. J., R. C. Meyers, P. M. Lang, K. A. Masarie, A. M. Crotwell, K. W. Thoning, B. D. Hall, J. W. Elkins, and L. P. Steele (2005), Conversion of NOAA atmospheric dry air CH_4 mole fractions to a gravimetrically prepared standard scale, *J. Geophys. Res.*, *110*, D18306, doi:10.1029/2005JD006035.

Etheridge, D. M., L. P. Steele, R. J. Francey, and R. L. Langenfelds (1998), Atmospheric methane between 1000 A.D. and present: Evidence of anthropogenic emissions and climatic variability, *J. Geophys. Res.*, *103*, 15,979–15,993.

Ferretti, D. F., et al. (2005), Unexpected changes to the global methane budget over the past 2000 years, *Science*, *309*, 1714–1717.

Frankenberg, C., J. F. Meirink, M. van Wheele, U. Platt, and T. Wagner (2005), Assessing methane emissions from global space-borne observations, *Science*, *308*, 1010–1014.

Fung, I., J. John, J. Lerner, E. Matthews, M. Prather, L. P. Steele, and P. J. Fraser (1991), Three-dimensional model synthesis of the global methane cycle, *J. Geophys. Res.*, *96*, 13,033–13,065.

Grenfell, A. L., D. T. Shindell, D. Koch, and D. Rind (2001), Chemistry-climate interactions in the Goddard Institute general circulation model: 2. New insights into modeling the pre-industrial atmosphere, *J. Geophys. Res.*, *106*, 33,435–33,451.

Haan, D., P. Martinerie, and D. Raynaud (1996), Ice core data of atmospheric carbon monoxide over Antarctica and Greenland during the last 200 years, *Geophys. Res. Lett.*, *23*, 2235–2238.

Haan, D., P. Y. Zuo, V. Gros, and C. A. M. Brenninkmeijer (2001), Photochemical production of carbon monoxide in snow, *J. Atmos. Chem.*, *40*, 217–230.

Hein, R., P. J. Crutzen, and M. Heimann (1997), An inverse modeling approach to investigate the global atmospheric methane cycle, *Global Biogeochem. Cycles*, *11*, 43–76.

Houweling, S., F. Dentener, and J. Lelieveld (2000), Simulation of preindustrial atmospheric methane to constrain the global source strength of natural wetlands, *J. Geophys. Res.*, *105*, 17,243–17,255.

International Panel on Climate Change (2001), *Climate Change 2001*, edited by J. T. Houghton et al., 881 pp., Cambridge Univ. Press, New York.

Johnson, C. E., D. S. Stevenson, W. J. Collins, and R. G. Derwent (2001), Role of climate feedback on methane and ozone studied with a coupled Ocean-Atmosphere-Chemistry model, *Geophys. Res. Lett.*, *28*, 1723–1726.

Kaplan, J. O. (2002), Wetlands at the Last Glacial Maximum: Distribution and methane emissions, *Geophys. Res. Lett.*, *29*(6), 1079, doi:10.1029/2001GL013366.

Keppler, F., J. Hamilton, M. Braß, and T. Röckmann (2006), Methane emissions from terrestrial plants under aerobic conditions, *Nature*, *439*, 187–191.

Khalil, M. A. K., and R. A. Rasmussen (1987), Atmospheric methane trends over the last 100,00 years, *Atmos. Environ.*, *21*, 2445–2452.

Kirschbaum, M. U. F., D. Bruhn, D. M. Etheridge, J. R. Evans, G. D. Farquhar, R. M. Gifford, K. I. Paul, and A. J. Winters (2006), A comment on the quantitative significance of aerobic methane release by plants, *Funct. Plant Biol.*, *33*, 521–530.

Koch, D., D. Jacob, I. Tegen, D. Rind, and M. Chin (1999), Tropospheric sulfur simulation and sulfate direct radiative forcing in the Goddard Institute for Space Studies general circulation model, *J. Geophys. Res.*, *104*, 23,799–23,822.

Kucera, M., A. Rosell-Mele, R. Schneider, C. Waelbroeck, and M. Weinelt (2005), Multiproxy approach for the reconstruction of the glacial ocean Surface (MARGO), *Quat. Sci. Rev.*, *24*, 813–819.

Martinerie, P., G. P. Brasseur, and C. Granier (1995), The chemical composition of ancient atmospheres: A model study constrained by ice core data, *J. Geophys. Res.*, *100*, 14,291–14,304.

Maslin, M., M. Owen, S. Day, and D. Long (2004), Linking continental-slope failures and climate change: Testing the clathrate gun hypothesis, *Geology*, *32*, 53–56.

Matthews, E. (2000), Wetlands, in *Atmospheric Methane: Its Role in the Global Environment*, edited by M. A. K. Khalil, pp. 202–233, Springer, New York.

Mickley, L. J., P. P. Murti, D. J. Jacob, J. A. Logan, D. M. Koch, and D. Rind (1999), Radiative forcing from tropospheric ozone calculated with a unified chemistry climate model, *J. Geophys. Res.*, *104*, 30,153–30,172.

Novelli, P. C., K. A. Masarie, and P. M. Lang (1998), Distributions and recent changes in carbon monoxide in the lower troposphere, *J. Geophys. Res.*, *103*, 19,015–19,033. (Available at www.cmdl.noaa.gov/ccgg/iadv)

Pavelin, E. G., C. E. Johnson, S. Rughooputh, and R. Toumi (1999), Evaluation of pre-industrial surface ozone measurements made using Schonbein's method, *Atmos. Environ.*, *33*, 919–929.

Peltier, R. W. (1994), Ice age paleotopography, *Science*, *265*, 195–201.

Prather, M., R. Derwent, D. Ehhalt, P. Fraser, E. Sanheuza, and X. Zhou (1995), Other tracer gases and atmospheric chemistry, in *Climate Change 1994*, edited by J. T. Houghton et al., pp. 73–126, Cambridge Univ. Press, New York.

Prather, M. J., et al. (2001), Atmospheric chemistry and greenhouse gases, in *Climate Change 2001*, edited by J. T. Houghton et al., pp. 239–287, Cambridge Univ. Press, New York.

Prinn, R. G., R. F. Weiss, B. R. Miller, J. Huang, F. N. Alyea, D. M. Cunnold, P. J. Fraser, D. E. Hartley, and P. G. Simmonds (1995), Atmospheric trend and lifetime of CH_3CCl_3 and global OH concentrations, *Science*, *269*, 187–192.

Rayner, N. A., D. E. Parker, E. B. Horton, C. K. Folland, L. V. Alexander, D. P. Rowell, E. C. Kent, and A. Kaplan (2003), Global analyses of sea surface temperature, sea ice, and night marine air temperature sine the late nineteenth century, *J. Geophys. Res.*, *108*(D14), 4407, doi:10.1029/2002JD002670.

Ridgewell, A. J., S. J. Marshall, and K. Gregson (1999), Consumption of atmospheric methane by soils: a process-based model, *Global Biogeochem. Cycles*, *13*, 59–70.

Rind, D., and D. Peteet (1985), Terrestrial conditions at the last glacial maximum and CLIMAP sea-surface temperature estimates: Are they consistent?, *Quat. Res.*, *24*, 1–22.

Rind, D., P. Demencal, G. L. Russel, S. Sheth, D. Collins, G. A. Schmidt, and J. Teller (2001), Effects of glacial meltwater in the GISS Coupled Atmosphere-Ocean Model: 1. North Atlantic Deep Water response, *J. Geophys. Res.*, *106*, 27,335–27,354.

Schaefer, H., M. J. Whiticar, E. Brook, V. Petrenko, D. Ferretti, and J. Severinghaus (2006), Ice record of $\delta^{13}C$ for atmospheric CH4 across the Younger Dryas–Preboreal transition, *Science*, *313*, 1109–1112.

Schimel, D., et al. (1996), Radiative forcing of climate change, in *Climate Change 1995: The Science of Climate Change, Second Assessment Report, International Panel on Climate Change*, edited by J. T. Houghton, pp. 65–131, Cambridge Univ. Press, New York.

Schmidt, G. A., et al. (2006), Present day atmospheric simulations using GISS ModelE: Comparison to in-situ, satellite and reanalysis data, *J. Clim.*, *19*, 153–192, doi:10.1175/JCL13612.1.

Shindell, D. T., and G. Faluvegi (2002), An exploration of ozone changes and their radiative forcing prior to the chlorofluorocarbon era, *Atmos. Chem. Phys.*, *2*, 363–374.

Shindell, D. T., J. L. Grenfell, D. Rind, C. Price, and V. Grewe (2001), Chemistry-climate interactions in the Goddard Institute for Space Studies general circulation model: 1. Tropospheric chemistry model description and evaluation, *J. Geophys. Res.*, *106*, 8047–8076.

Shindell, D. T., G. Faluvegi, and N. Bell (2003), Preindustrial-to-present-day radiative forcing by tropospheric ozone from improved simulations with the GISS chemistry-climate GCM, *Atmos. Chem. Phys.*, *3*, 1675–1702.

Shindell, D. T., G. Faluvegi, and L. K. Emmons (2005), Inferring carbon monoxide pollution changes from space-based observations, *J. Geophys. Res.*, *110*, D23303, doi:10.1029/2005JD006132.

Sowers, T. (2006), Late Quaternary atmospheric CH_4 isotope record suggests marine clathrates are stable, *Science*, *311*, 838–840.

Spivakovsky, C. M., et al. (2000), Three-dimensional climatological distribution of tropospheric OH: Update and evaluation, *J. Geophys. Res.*, *105*, 8931–8980.

Valdes, P. J., D. J. Beerling, and C. E. Johnson (2005), The ice age methane budget, *Geophys. Res. Lett.*, *32*, L02704, doi:10.1029/2004GL021004.

Walter, B. P., M. Heimann, and E. Matthews (2001), Modeling modern methane emissions from natural wetlands: 1. Model description and results, *J. Geophys. Res.*, *106*, 34,189–34,206.

Webb, R. S., D. H. Rind, S. J. Lehman, R. J. Healy, and D. Sigman (1997), Influence of ocean heat transport on the climate of the Last Glacial Maximum, *Nature*, *385*, 695–699.

Whalen, S. C., and W. Reeburgh (1992), Interannual variations in tundra methane emission: A 4-year time series at fixed sites, *Global Biogeochem. Cycles*, *6*, 139–159.

World Meteorological Organization (1999), *Scientific Assessment of Ozone Depletion*: *1998*, Geneva.

E. J. Brook, Department of Geosciences, Oregon State University, Corvallis, OR 97331-5506, USA. (brooke@geo.oregonstate.edu)

S. L. Harder, School of Earth and Environmental Sciences, Washington State University, 14204 NE Salmon Creek, Vancouver, WA 98686, USA. (harders@vancouver.wsu.edu)

G. A. Schmidt and D. T. Shindell, NASA Goddard Institute for Space Studies and Center for Climate Systems Research, Columbia University, 2880 Broadway, New York, NY 10025, USA. (gschmidt@giss.nasa.gov; dshindell@giss.nasa.gov)